LAWRENCE
LIVERMORE
NATIONAL
LABORATORY

LLNL-JRNL-431628

High-energy x-ray backlighter spectrum measurements using calibrated image plates

B. R. Maddox, H.-S. Park, B. A. Remington, N. Izumi, S. Chen, C. Chen, G. Kimminau, Z. A. Ali, M. J. Haugh, Q. Ma

May 13, 2010

Review of Scientific Instruments

Disclaimer

High-energy x-ray backlighter spectrum measurements using calibrated image plates

B. R. Maddox, H.-S. Park, B. A. Remington, and N. Izumi

Lawrence Livermore National Laboratory, Livermore CA, 94550, USA

S. Chen, C. Chen

University of California, San Diego CA, 92093-0418, USA

G. Kimminau

University of Oxford, UK

Z. A. Ali and M. J. Haugh

National Security Technologies, LLC.

Q. Ma

DND-CAT, Argonne National Lab, Argonne IL 60439-4857

The x-ray spectrum between 18keV and 88 keV of a petawatt laser generated x-ray backlighter was measured using a six-channel spectrometer consisting of a series of differential filter pairs, also known as Ross pairs, in front of calibrated image plates. The image plates were calibrated using a Tungsten anode source and an absolutely calibrated Ge detector. The resulting calibration curve was successfully fit to a multi-region energy absorption model and applied to the design of the Ross pair spectrometer. It is known that spontaneous emission of photoluminescence by thermal recombination results in lower sensitivity as a function of time from exposure. This effective image fade rate was measured from 5 to 10^4 minutes after exposure to account for variations between laser shot time and image plate scan time. Measurements of the conversion efficiency of laser light into Silver Kα from a petawatt laser target using the Ross pair spectrometer is consistent with previously measured values and with single photon counting CCD measurements. The resolution (modulation transfer function, or MTF) of the image plate system was also measured for radiographic applications.

Introduction

High-energy radiography using petawatt laser ($>10^{15}$ W/cm^2) driven x-ray backlighters is a premier tool for diagnosing internal confinement fusion (ICF) and other high energy density (HED) experiments where high x-ray brightness and a very short pulse duration are desirable [2]. In these experiments, a burst of x-rays is generated when the high intensity laser strikes a small, typically metal, foil through collisions between atoms in the foil and relativistic "hot" electrons produced by the laser-matter interaction at the surface of the foil. The x-rays emitted are a mix of characteristic x-rays and brehmstrallung radiation that can extend well past 1 MeV. Quantitative analysis of the resulting radiographs requires a detailed knowledge of both the x-ray source and the detector. However, the combination of the harsh laser environment and the exceptionally broadband source make spectral measurements challenging.

Differential filters, also known as Ross pairs, coupled with image plate detectors can provide a robust, cost effective way of characterizing the broadband x-ray spectrum emitted from petawatt laser targets. A Ross pair is a pair of filter materials, typically consisting of adjacent atomic numbers, whose thicknesses have been chosen such that the transmitted spectra are identical except for the narrow energy band between their respective K-edges [13]. The difference between the transmitted signals is then proportional to the x-ray flux in that band. While the spectral resolution may be coarse, differential filtering has an advantage over other popular methods of high energy x-ray spectroscopy, such as a crystal spectrometer, in that the

measured signal intensity is much greater thanks to the non-dispersive signal collection. With proper design, the data analysis of Ross pair data is also much simpler compared to other filter/dosimeter spectrometers [15]. Image plates are ideal for measuring the x-ray signal intensity behind the filters as they are robust against EMP, are linear with dose over a much wider dynamic range (>10^5) than film emulsion, and, unlike film, do not require a complicated chemical development process [1].

This paper describes an x-ray spectrum measurements using a Ross pair spectrometer coupled to calibrated images plates and is divided into two main parts. Part I describes the various calibration measurements of the image plate detectors including spectral sensitivity, x-ray absorption measurements, image fade rate, and system resolution. Part II describes the design of the spectrometer and the results of spectrum measurments of a Ag foil petawatt backlighter target including laser energy to Kα conversion efficiency measured by the spectrometer compared to a measurement obtained by single photon counting using a Charge Coupled Device (CCD).

I. Calibration of image plates

Image plates (IPs) are based on an x-ray sensitive layer made from BaF(Br,I):Eu^{2+} phosphor crystals suspended in a plastic binder. Specifications for the two types of Fuji™ brand plates calibrated in this study, SR and MS-type, are shown in Table I and are a compilation of information from Fuji and experimental measurements [4]. Here, SR stands for "super-resolution" and MS stands for "more-sensitive". Absorbed x-rays ionize the Eu^{2+} and generate photoelectrons that become trapped in lattice defects created by the absence of halogen ions in

the BaF crystals (called F- or color-centers). The image is read out by irradiating the IP with a (red) laser beam (λ=632.8 nm), causing recombination and reduction of the Eu^{3+} back to Eu^{2+} and the release of a (blue) photon. This light is called photo-stimulated luminescence (PSL) and is collected by a photomultiplier tube. Because the latent image is stored in metastable F-centers, thermal activation can also cause recombination, fading the stored image with time.

	MS			SR		
	Composition	**Density (g/cm^3)**	**Thickness (μm)**	**Composition**	**Density (g/cm^3)**	**Thickness (μm)**
Mylar Layer*	$C_{10}H_8O_4$	1.64	9	$C_{10}H_8O_4$	1.49	8
Sensitive Layer*	$BaFBr_{0.85}I_{0.15}$:Eu	3.18	124	BaFBr:Eu	3.07	112
Back Layer	Plastic	1.4	12	Plastic	1.4	12
Base Layer	$C_{10}H_8O_4$	1.4	190	$C_{10}H_8O_4$	1.4	190
Ferromagnetic Layer	MnO, ZnO, Fe_2O_3 + plastic	3.0	80	MnO, ZnO, Fe_2O_3 + plastic	3.0	80
Back protective layer	$C_{10}H_8O_4$	1.4	25	$C_{10}H_8O_4$	1.4	25

Table I. Composition of Fuji MS and SR image plates. These numbers represent the best guess composition for layers other than the Mylar and sensitive layers. *Density of and thickness reported in Ref. [4].

Both the SR and MS plates have a thin layer of Mylar, protecting the sensitive layer, and a ferromagnetic backing layer. Additionally, SR-type IP has a blue dye mixed into the sensitive layer. The blue dye in the sensitive layer of SR plates reduces scattering of the irradiating laser and emitted PSL, increasing the resolution. The addition of blue dye, however, lowers the overall sensitivity of the system by absorbing some of the red readout laser light.

A Fuji model FLA7000 flatbed image plate scanner was used to read the image plate data. Image plates are loaded into the scanner on a magnetic tray that adheres to the ferrite backing layer of the IP. The magnetic tray of the FLA7000 allows arbitrarily sized plates to be scanned, which is of considerable convenience when experiments involve image plate detectors of various size, shape, and number. The FLA7000 uses a rotating prism in the readout optics that effectively reads an entire line of resolution at a time, decreasing both readout time and noise level compared to x-y rastering optics. The decrease in readout time is especially important for minimizing fade during the scanning process itself.

Absorption measurements

In many experiments it is advantageous to stack multiple image plates to create a layered detector, so to confirm the composition of the plates and to facilitate stacking of plates, the x-ray absorption spectra of MS and SR image plates were measured at the Sector 5 DND-CAT BM-D bending magnet beam line of the Advanced Photon Source at Argonne National Laboratory. This beam line is capable of delivering 20 to 100 keV monochromatic x-rays at a high flux level. Ionization chambers were used to measure the x-ray flux in front, and behind the image plates as a function of x-ray energy. The absorption fraction as a function of x-ray energy, *A(E),* was then calculated using

$$A(E) = \frac{I'}{I} \times \frac{I_0}{I'_0} \qquad \text{Eq. (1)}$$

where *I'* and *I* are the flux values behind the IP plane with and without the image plate and I'_0 and I_0 are the flux values in front of the IP plane with and without the image plate, respectively.

Here, *A(E)* refers to the absorption fraction through the entire plate, not just the x-ray sensitive region.

Figure 1 shows the absorption spectra of MS and SR plates. Also shown is the calculated absorption fraction, given the density and chemical formulas from Table I. For the SR image plate, the experimental and calculated absorption fractions agree to within 1%. However, the calculated absorption in MS plate is 2 to 3% higher than the measured results when using the values given in the literature for the composition and thickness [4]. A calculated absorption curve using an active layer thickness of 115 μm, which is the factory specified value, matched the experimental data to better than 1%.

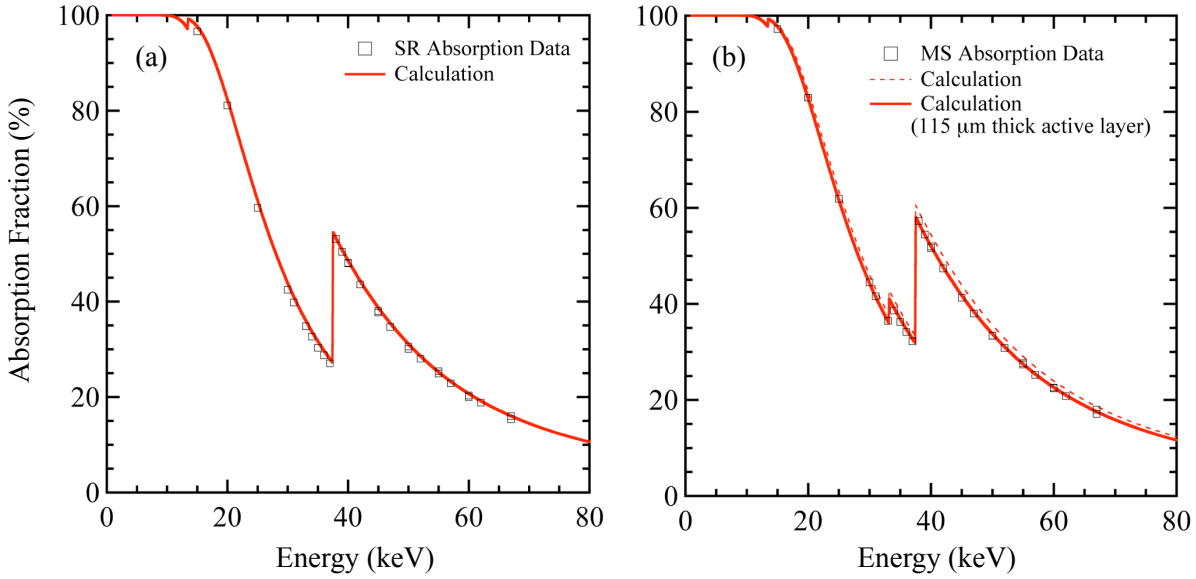

Figure 1. Absorption spectrum and calculated absorption curve for (a) SR and (b) MS image plates showing the absorption edges of Br (13.474 keV), Ba (37.44 keV), and I (33.170 keV, MS only). Good agreement is obtained using the SR plate composition shown in Table I. For the MS plate, the factory specified thickness of 115 μm for the active layer agrees well with the experimental data.

Image plate fade curve

Detailed knowledge of the image fade curve is critical for quantitative applications where the plates may be scanned at varying time after exposure. Previous studies have shown that the fade rate of image plates is a function of IP composition, radiation type and energy, temperature of the IP, and model of the scanner [5]. Each radiation type typically introduces an exponential component to the overall fade curve. A mix of alpha- and gamma rays produces a three-component exponential fade function [5,7]. A single component exponential form was obtained in a previous study [4] using x-rays. However, only fade times up to 300 minutes were measured, whereas time constants up to $7x10^5$ minutes have been reported using Fuji BAR-UR image plates [6].

In this study, fading rates of Fuji MS and SR image plates exposed to 22.2 keV x-rays were measured by performing a series of exposures using a ^{109}Cd radioactive sealed source and scanning each plate from 5 minutes to 10,000 minutes after exposure. Exposures were kept short, 60 seconds, to eliminate the effect of fade on the exposure itself. Ambient temperature was kept at 68 +/- 1° F. The resulting fade rate is plotted in Figure 2, normalized to the PSL level t=0. A single component exponential was unable to reproduce the late-time fade characteristics, so a two-component exponential of the form

$$F(t) = y_0 + A_1 e^{-\frac{t}{\tau_1}} + A_2 e^{-\frac{t}{\tau_2}} \qquad \text{Eq (2).}$$

was used to fit the data. Here, t is the time elapsed after the end of the exposure and A_i, τ_i are the amplitude and time constants. The fits to the experimental data are also shown in Fig. 2.

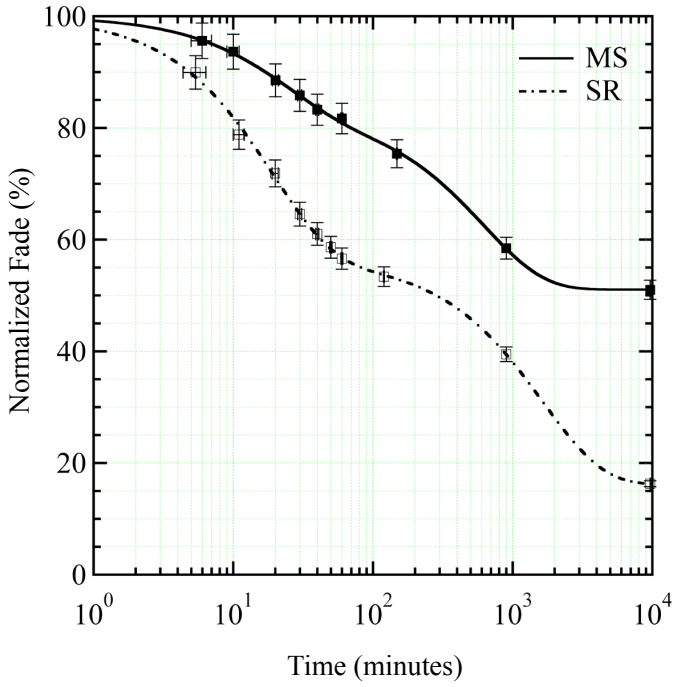

Figure 2. Fading rate of MS and SR image plate material exposed to 22.162 keV x-rays for 60 sec and stored at 68° +/-1 F and normalized to t=0. The solid and dashed curves show two-component exponential fits to the MS and SR data points, respectively.

The fit parameters obtained, summarized in Table II, are in qualitative agreement with those of Ref. [4] and show that the initial fade component for MS is slower than SR and that the amplitude of the fade for MS is lower than for SR. However, the long-component time constants τ_2=615.9±42.1 and τ_2=1641.5±152.3 minutes for MS and SR image plates demonstrate the importance of fade measurements at sufficiently long times. Additionally, the short-component time constants τ_1=23.0±2.7 and τ_1=18.9±1.5 minutes for MS and SR image plates obtained in this study are smaller by at least a factor of 3 than the single-component time constants previously measured. This is also likely due to the larger range of fade times sampled here and the introduction of a second, long time-constant fade component.

Image Plate Type	A_1 (PSL)	τ_1 (min)	A_2 (PSL)	τ_2 (min)	y_0 (PSL)
MS	0.175±0.009	23.0±2.7	0.315±0.009	615.9±42.1	0.511±0.005

SR	0.436±0.016	18.9±1.5	0.403±0.013	1641.5±152.3	0.162±0.010

Table II. Two-component exponential fit parameters to the image plate fade data shown in Fig. 2 for an ambient temperature of 68° +/-1 F.

Image plate spectral response calibration

The spectral sensitivity of the FLA7000 system using MS and SR image plates was measured at the High Energy X-ray (HEX) facility, located at NSTec LLC. In Livermore, CA. The HEX facility uses a Yxlon Tungsten x-ray tube to irradiate various foil targets. The result is characteristic line emission superimposed over a Brehmstrallung radiation background. The x-rays produced by the foil targets were passed through an 11 mm diameter collimator and an absorption edge filter. The x-ray spectrum at the image plate plane, located 1 m from the foil target source, was measured using an absolutely calibrated Canberra Ge detector before and after each exposure and the total flux was reproducible to better than 1%. Because the characteristic lines were superimposed over a Bremstrahlung radiation background, a weighted mean of the measured spectra was used to define the photon energy for each foil fluorescer and the x-ray energy error defined as the weighted standard deviation of the corrected spectrum. This error increases with energy due to the increasing energy spacing between characteristic lines. A typical spectrum obtained using a Silver fluorescer is shown in Fig. 3. The lines above 30 keV are due to multiple Ag Kα/β photon events and are added to the main Kα and Kβ peaks when calculating the weighted mean x-ray energy. The low energy peaks are a complicated mixture of multiple-photon events including W L-emission, Si K-emission and Ag-L emission, but contribute little to the total energy deposited in the IP.

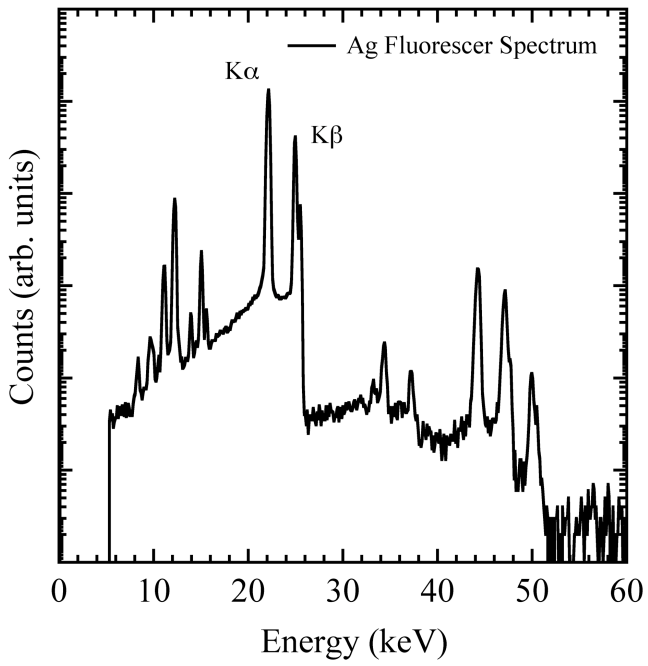

Figure 3. Spectrum generated by the HEX facility using a Silver fluorescer showing the characteristic Kα and Kβ lines. The lines above 30 keV are multi-photon events that are added to the main Kα and Kβ peaks during the spectral analysis. The low energy peaks are a complicated mixture of multiple-photon events including W L-emission, Si K-emission and Ag-L emission.

Two image plates of each type, MS and SR, were studied and will be referred to as plates A and B. The SR plates were from the same batch (same plate serial number) while the two MS plates were from different batches. Each image plate was erased for a minimum of 15 minutes before being loaded into an Aluminum cartridge, covered with a thin, light-tight carbonized Kapton film, and exposed to the x-ray source for 60s. The plates were then scanned 30 minutes after exposure, using a 50 μm scanning step size, medium sensitivity (S4000), and 16-bit image dynamic range settings. This procedure was repeated for each of the four image plates at each x-ray energy.

Figure 4 shows the resulting spectral sensitivity, or PSL per incident photon, for SR and MS image plates. The error in the sensitivity measurement was dominated by the error in the measured incident x-ray flux due to misalignment of the Ge detector with the center of the image plate. Thus, vertical error bars were derived from the standard deviation of PSL measurements over a 1 cm^2 region in the center of the IP, which is likely an overestimate of the Ge detector alignment error. The sensitivities of the two SR plates were within <1% of each other. However, the sensitivity of MS plate A was consistently 13% higher than MS plate B throughout the entire energy range measured. This information, coupled with the absorption measurement implies batch-to-batch variations in the thickness of the sensitive layer. Thus, the sensitivity data in Fig. 4 for MS plate B was multiplied by 1.13.

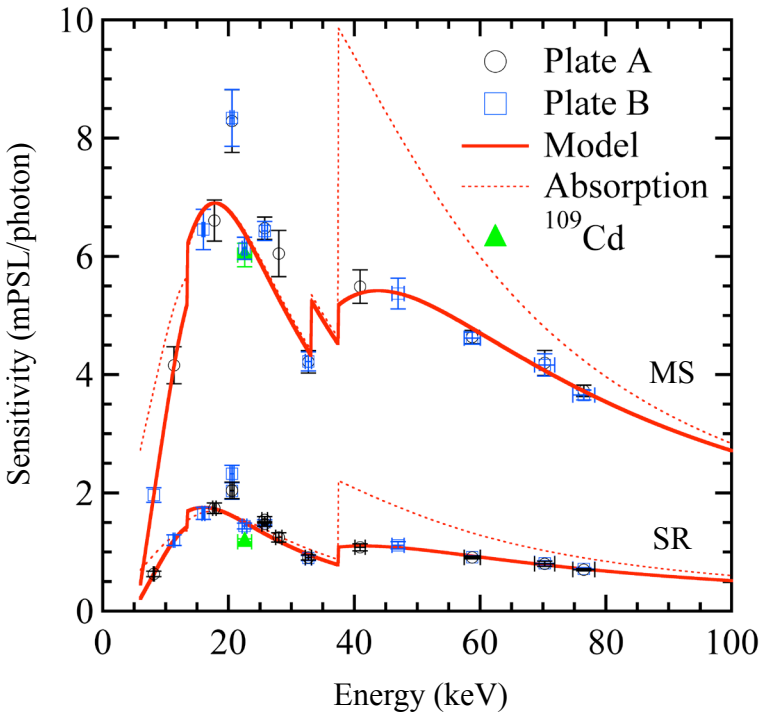

Figure 4. Sensitivity of the FLA7000 IP system using MS and SR image plates scanned at 50 µm step size 30 minutes after exposure. The dotted curves show a theoretical sensitivity curve assuming a fixed value for the energy absorbed per PSL. The solid curves show the fits to a sensitivity model

which assumes a different value for the energy absorbed per PSL in each energy region, separated by absorption edges in the sensitive layer materials.

The PSL measured by the system is proportional to the energy deposited in the sensitive layer of the IP. A calculated phosphor absorption model (dotted curves) that assumes a fixed linear constant of proportionality over the entire energy region sampled is shown in Fig. 4 for MS and SR image plates, scaled to fit the 15 to 35 keV region of the data. It is clear that this simple model does not fit the data, especially above the Ba L- and K-edges where significant energy loss due to fluorescence can occur. A more realistic model of the IP sensitivity is also shown (solid curves) that breaks the sensitivity into 4 regions, separated by the Ba-L (5.987 keV), Br-K (13.474), and Ba-K (37.441 keV) edges [4,8]. This model also assumes that the measured PSL is linearly proportional to the absorbed energy, but the constants of proportionality are different in each energy. If $\eta(E)$ is the absorption fraction in the sensitive region of the IP

$$\Omega(E) = \eta(E) \times \begin{cases} (m_I \times E + b_I) & \text{if } 0 \le E < 5.987 \text{ keV} \\ (m_{II} \times E + b_{II}) & \text{if } 5.987 \le E < 13.474 \text{ keV} \\ (m_{III} \times E + b_{III}) & \text{if } 13.474 \le E < 37.441 \text{ keV} \\ (m_{IV} \times E + b_{IV}) & \text{if } E \ge 37.441 \text{ keV} \end{cases} \qquad \text{Eq. (3)}$$

where $\Omega(E)$ is the sensitivity (PSL/incident photon) and m, $\mathbf{b}$ are the linear fit coefficients in the 4 energy regions. The coefficients for Regions II, III, and IV were determined by performing linear fits to the sensitivity divided by the absorption fraction in each of the energy regions. The coefficients for Region I could not be determined as no data was obtained below 8.128 keV. The calculated sensitivity curves using the model described in Eq. (3) are also shown in Fig. 4, starting with Region II, and the coefficients are given in Table III. Also shown in Fig. 4 are two

single-point calibrations performed using a ^{109}Cd sealed source with different image plates and scanned on a different FLA7000 scanner. Both of these data points are within experimental error of the model sensitivity curves. It is important to keep in mind that the absolute sensitivity of the image plate system is dependent on the scanner type and that the numbers presented in this study only apply to plates scanned using an FLA7000 scanner. However, the shape of the sensitivity curve should remain the same assuming the same laser wavelength. Thus, a single point calibration should be sufficient to apply the sensitivity curves presented here to systems using a different model scanner

Coefficient	Region		
	II	III	IV
m (SR) (PSL/eV)	1.943×10^{-7}	9.146×10^{-8}	1.271×10^{-7}
b (PSL/photon)	-9.475×10^{-4}	5.178×10^{-4}	-2.596×10^{-3}
m (MS) (PSL/eV)	7.098×10^{-7}	4.446×10^{-7}	5.658×10^{-7}
b (PSL/photon)	-3.789×10^{-3}	3.745×10^{-4}	-1.205×10^{-2}

Table III. Linear fits to the IP sensitivity model in the energy regions: 5.987->13.474 (region II), 13.474->37.441 (region III), >37.441 (region IV) for SR and MS image plate.

The MS image plates were more sensitive than the SR image plates by factors ranging from 3.13 at 8.128 keV to 5.25 at 76.506 keV, as shown in Fig. 5. The lower sensitivity of the SR image plate is due to the blue dye in the active layer that absorbs some of the red readout laser light, limiting lateral scattering and increasing the spatial resolution. Additionally, the introduction of an absorbing medium decreases the penetration depth of the readout laser into the

sensitive layer of SR plate. This accounts for the relative increase in MS sensitivity with increasing energy.

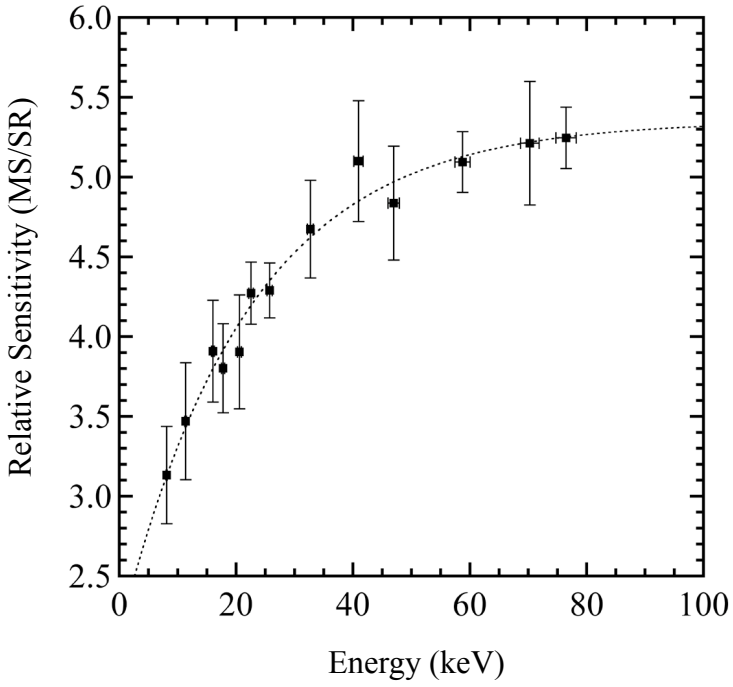

Figure 5. Relative sensitivity of MS to SR image plate, scanned at 50 μm step size, as a function of photon energy. The dotted line shows an exponential fit to the data.

The sensitivity of the scanning system as a function of scanning step size was investigated using a reference ^{14}C source used by Fuji for factory calibration. The ~2 cm diameter source was placed directly in contact with the image plates and the plates were exposed for 5 minutes and scanned 20 minutes after that. This is the same procedure Fuji has developed for factory calibration of the FLA7000 image plate system and should yield 100 PSL/mm^2 when using MS image plate scanned using a 50 μm step size. This procedure was repeated using both MS and SR image plate at 25, 50 and 100 μm step sizes, as well as the 3 difference sensitivity settings. All three sensitivity settings gave the same value at a given step size, however the amount of PSL/mm^2 obtained increased with step size. This is due to the fixed laser spot size of

~70 μm used by the FLA7000 regardless of the scanning step. Thus, the sensitivity of the system is reduced for step sizes smaller than the spot size due to overscan. Table IV shows the sensitivity scaling normalized to 50 μm step size. It is interesting to note that the relative difference in sensitivity between the different step sizes is smaller for SR plate than for MS plate, presumably due to the reduced scattering in SR plate. The sensitivity curve shown in Fig. 4 should be modified by the values in Table IV to derive the true sensitivity at step sizes other then 50 μm and by the fade curve in Fig. 2 for scan times other than 30 minutes after exposure.

IP Type	Sensitivity Multiplier		
	25 um	50 um	100 μm
MS	0.67	1.0	1.38
SR	0.79	1.0	1.13

Table IV. Sensitivity scaling as a function of scanning step size for MR and SR image plate. The sensitivity curve in Fig. 4 should be multiplied by these values to derive the true sensitivity curve for step sizes other than 50 μm.

Image plate resolution

For completeness, and for radiographic applications requiring high resolution, the MTF of the FLA7000 IP system at 22.2 keV using MS and SR plates was also measured at 25, 50, and 100 um scanning step size at the HEX facility using the same experimental setup described above but with a Pb resolution chart in contact with the image plates. The resolution chart was manufactured by FLUKE Biomedical and consists of a series of square resolution bars of increasing spatial frequency from 0.25 lp/mm to 10 lp/mm made from 50 μm thick Pb encased in plastic. The image plate plane was moved to 2 m from the fluorescer to increase the degree of flatness across the roughly 6.3 cm long resolution chart. Figure 6 shows a radiograph of the resolution chart taken using 22 keV x-rays and scanned at 25 μm step size.

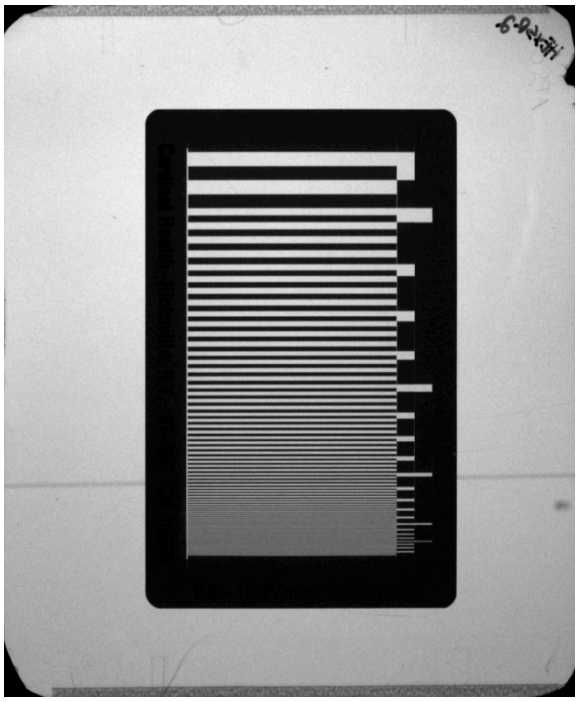

Figure 6. Radiograph of a Pb resolution chart taken using the SR IP at 22.565 keV and scanned at 25 μm scanning step size. The rotating prism axis is vertical. The faint horizontal line is due to debris on the rotating prism.

The modulation transfer function, or MTF(*f*), was measured by obtaining the contrast transfer function, or |CTF(*f*)|, which is defined as

$$\left|CTF(f)\right| = \frac{I_{\max} - I_{\min}}{I_{\max} + I_{\min}} \qquad \text{Eq. (4)}$$

where I_{max} and I_{min} are the maximum and minimum PSL values at a particular spatial frequency, *f*, in the Pb resolution chart image. The CTF(*f*) can be related to the MTF(*f*) through a Fourier analysis after fitting the measured |CTF(*f*)| with a model line spread function, or LSF(*x*) [1]. A

single-Gaussian line spread function was unable to reproduce the data, whereas a double-Gaussian LSF(x) produced a good fit to the experimental |CTF(f)| data. The second Gaussian component is likely due to scattering in the sensitive layer of the IP and is lower in SR relative to MS. The line spread function was also be obtained directly by taking the derivative of the edges of the Pb resolution chart. Good agreement was seen between the two methods.

The MTF(f) of SR and MS IP is compared in Fig. 7(a) and 7(b), respectively, for 25, 50, and 100 μm scanning step size along the direction perpendicular to the rotating prism of the image plate scanner. At 100 μm step size, no difference in MTF(f) is seen between the two types of plate. The resolution using SR plate continues to increase all the way down to 25 μm step size. In contrast, the MTF(f) using MS plate is the same for the 50 μm and 25 μm step sizes. This implies that scattering in the sensitive layer of MS plate is the limiting factor in resolution, whereas the scanner is the limiting factor when using SR plate. Also shown in Fig. 7 are |CTF(f)| data taken by Seely et al.[9] using a Logos DCR810 IP scanner at 47 μm scanning step size and Gales et al.[10] using a Fuji BAS2500 IP scanner at 50 μm scanning step size which, to first approximation, can be compared to the MTF(f) data presented here. For MS IP the data from Ref. [9] matches the current study well at mid frequency but diverges a bit at low and high frequency. However, the data from Ref. [9] and Ref. [10] using SR plate shows a higher MTF(f) than the current study for all spatial frequencies, consistent with SR plate resolution being scanner-limited.

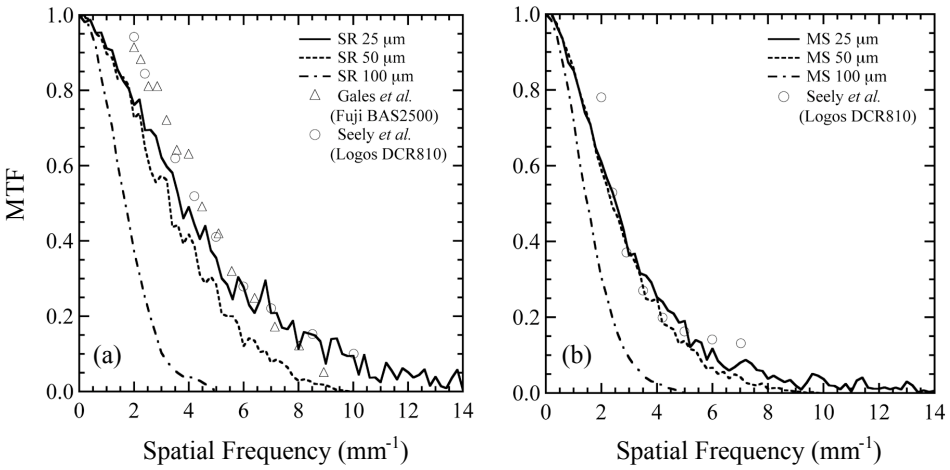

Figure 7. Modulation transfer function of the Fuji FLA7000 system using SR(a) and MS(b) plates exposed to 22.565 keV x-rays and scanned at 25, 50, and 100 μm scanning step size and perpendicular to the rotating prism. Also shown is |CTF(*f*)| data from Seely *et al.*[9] and Gales *et al.*[10] using a Logos DCR810 scanner at 47 μm step size and a Fuji BAS2500 at 50 μm step size, respectively.

A comparison of the MTF(*f*) using SR image plate, scanned at 50μm step size, along the two different scan directions is presented in Fig. 8. A decrease in resolution is seen in the direction parallel to the rotating prism scanning at high exposure level (>1000 PSL/mm^2). This effect was not seen at a low exposure level of ~50 PSL/mm^2. This decrease in resolution was seen for both types of plates at 25, and 50 μm scanning step size. At 25 μm pixel size, the scan time between adjacent pixels along the high-speed rotating prism scanning direction of ~ 1 μs is comparable to the 0.8 μs PSL lifetime [11]. Thus, the decrease in resolution along this direction at high PSL level is due to luminescence bleeding from adjacent pixels. This effect was not seen along the direction perpendicular to the rotating prism where the scan time between adjacent pixels is orders of magnitude longer in this direction. This effect should also diminish at larger step sizes as the speed of the rotating prism does not change. Indeed, at 100 μm step size where the scan time is 4 times longer than at 25 μm the MTF(*f*) was the same along both scanning directions for both types of plate.

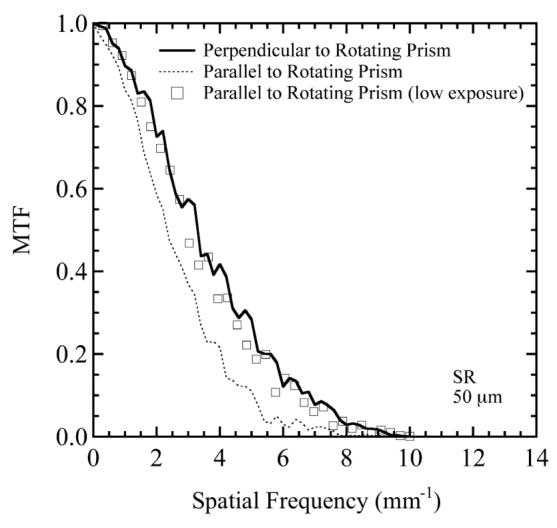

Figure 8. Modulation transfer function the FLA7000 system using SR plate at 50 μm scanning step size. Lines show |MTF(*f*)| derived from images at high exposure level (>1000 PSL/mm^2). Dashed line is parallel to the rotating prism direction. Solid line is perpendicular to the rotating prism direction. Open squares show |MTF(*f*)| parallel to the rotating prism direction at a low exposure level (50 PSL/mm^2).

II. Ross pair spectrometer

The IP calibration described in Part I was used to design a Ross pair spectrometer to measure the absolute high-energy x-ray spectrum from a Ag petawatt laser backlighter foil between 18 keV and 88 keV using 6 filter pairs (12 channels). A schematic of the setup is shown in Fig. 9. The spectrometer consists of a 25 um thick Ta mask with twelve 6 mm diameter holes laser cut in a circular pattern and backed by an MS image plate. Each of the holes acts as a single, isolated channel with the filters secured over the holes using 25 um thick Kapton tape. A large, 20 mm diameter circular hole was cut in the center of the Ta mask to allow the spectrometer to be placed in-line with other diagnostics, such as a single photon counting CCD camera. The entire assembly, measuring 81mm x 100mm, was housed in an Al clamshell cartridge covered in light-tight black Kapton-CB. Without the Ta mask, the areas of the image plate outside of the filter channels would saturate and contaminate the filtered areas with background PSL signal. Four additional 6 mm diameter holes along with one 1 mm diameter

fiducial hole were cut to allow indexing of the Ross pair filter channels and the placement of secondary filters, such as radiographic calibration steps.

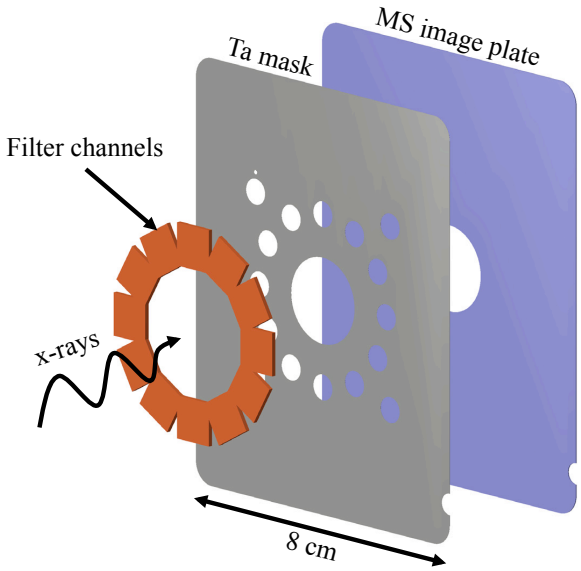

Figure 9. Schematic drawing of the Ross pair spectrometer assembly consisting of a 25 μm thick Ta mask with 12 filter channels secured over 6 mm diameter holes and backed by an MS-type image plate.

The difference in signal level between behind the two filters of a single Ross pair can be written explicitly as

$$\Delta PSL = C\left(\int_0^\infty \Phi(E)S(E)T_1(E)dE - \int_0^\infty \Phi(E)S(E)T_2(E)dE\right) \qquad \text{Eq. (5)}$$

where C is a geometric constant, $S(E)$ is the inident x-ray spectrum, $\Phi(E)$ is the image plate sensiticity (see Fig. 4), and $T_1(E)$ and $T_2(E)$ are the total transmissions through the two different filters, For perfect transmission match outside of the pass band, marked by the K-edges of the two filters E_1 and E_2, Eq. 5 can be simplified and rearranged to solve for S_{Eavg}, assuming that the spectrum is constant within the pass band

$$S_{Eavg} = \frac{\Delta PSL}{C\int_{E_1}^{E_2} \Phi(E)\left(T_1(E) - T_2(E)\right)dE} \qquad \text{Eq. (6)}$$

where S_{Eavg} is in the units of photons per energy bin at E_{avg}, or the average energy between E_1 and E_2. Proper selection of filter thicknesses can make the integrand in Eq. (6) a constant between E_1 and E_2. In this case, S_{Eavg} takes on the simple form

$$S_{Eavg} = \frac{\Delta PSL}{C \times R \times \Delta E} \qquad \text{Eq. (7)}$$

where R is defined as the "residual sensitivity" and is just the difference in transmission between the two filters multiplied by the image plate sensitivity at E_{avg}. The filter thicknesses for the Ross pair spectrometer were chosen such that the integrand in Eq. (5) was reasonably constant for all filter pairs while minimizing the contribution to ΔPSL from energies outside of the Ross pair pass band. This secondary metric, χ was calculated assuming an x-ray spectrum measured from a Ag petwatt backlighter on the Omega EP laser using a filter stack spectrometer [15].

The residual sensitivities and final filter materials and thicknesses are given in Fig. 10 and Table V, respectively. Also shown in Table V are the χ values calculated for each filter pair. Filter pairs were chosen based on commercially available materials and thicknesses. A low-Z material, in this case Aluminum, was added to the low-Z filter channel in each Ross pair to fine-tune the absorption when ideal filter thicknesses were not available [14]. The actual filter thicknesses were measured using a Heidenhain thickness gauge. The residual sensitivities given in Fig. 10 and Table V are calculated assuming MS image plates scanned 30 minutes after exposure and with a 50 um step size. It is important to note that the lowest energy pair, Zr-Mo (channels 1-2), is very sensitive to changes in filter thickness and that this resulted in a large χ.

Channel	Filter (um)	Energy Range (keV)	χ (%)	R (mPSL/γ)
1	Zr (35) Al (10)	17.99 – 19.99	73.7	7.18
2	Mo (19)			
3	Mo (38) Al (10)	19.99 – 24.35	0.2	5.53
4	Pd (26)			
5	Pd (60) Al (98.5)	24.35 – 29.20	1.2%	3.77
6	Sn (84)			
7	Sn (84) Al (441.5)	29.20 – 50.24	9.8%	2.44
8	Gd (50)			
9	Gd (250) Al (1007)	50.24 – 67.41	1.6%	2.67
10	Ta (92.5)			
11	Ta (221) Al (1007)	67.41 – 88.01	4.8%	1.84
12	Pb (246)			

Table V. Filter materials and thicknesses along with their pass band energy range, error metic χ, and the residual sensitivity *R*.

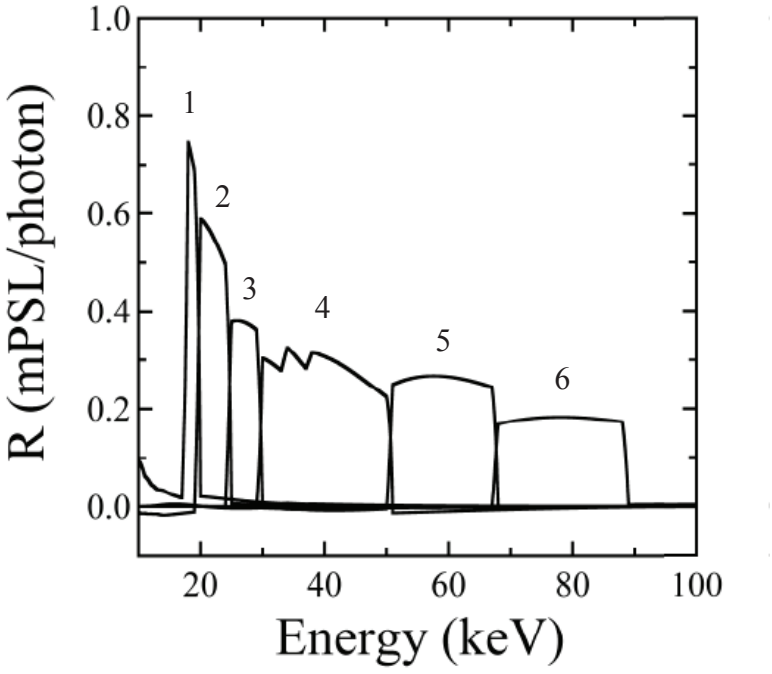

Figure 10. Residual sensitivity, *R*, as a function of energy for the 6 Ross pairs given in Table V.

Absolute X-ray spectrum and conversion efficiency measurements

The absolute x-ray spectrum Kα conversion effieicncy of a Ag petawatt target was measured using the Ross pair spectrometer and compared to single photon counting using a Spectral Instruments SI800 CCD camera [12]. Here, the conversion efficiency is defined to be the ratio of the total energy emitted as Kα photons yto the incident laser energy. The target was a 250 μm diameter, 12 μm Ag disc irradiated using the Titan laser at LLNL. The laser pulse energy was 296.6 J with a duration of 40 ps and focused to a spot size of 30 μm, resulting in an on-target intensity of 1.05×10^{18} W/cm^2. The Ross pair spectrometer was placed at a distance of 1.150 m along the same line-of-sight as the CCD camera, which was placed at a distance of 5.006 m and filtered with 35 μm of Mo to try and reduce the exposure level on the CCD to the single photon counting level.

Two different histograms of the resulting CCD image are plotted in Fig. 11, a standard histogram and a single pixel even histogram that rejects multiple pixel events. The standard histogram shows the Kα and Kβ peaks superimposed over a broad background of multiple pixel events [12]. The single event histogram gives a better representation of the low energy portion of the spectrum, revealing also the Mo K-edge. The exposure level, defined as the fraction of pixels with a signal above 3 time the background FWHM, on the CCD was 21%. At this exposure level and for monochromatic 22 keV x-rays, the counting efficiency of both histograms is reduced by ~50% compared to an ideal single photon counting exposure of 1% [12]. Using the histogram counting efficiencies from Ref. [12] the conversion efficiency into Kα becomes 2.4×10^{-4} using the standard histogram method and 3.0×10^{-4} using the single even histogram method.

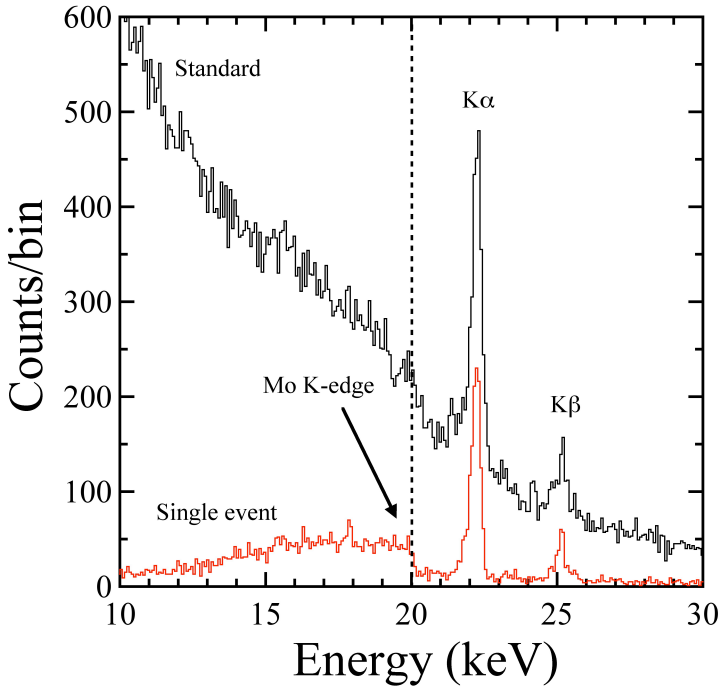

Figure 11. Standard and single event histograms of single photon counting CCD image showing Ag Kα and Kβ x-ray peaks at 22.162 and 24.942 keV. The broad sloping background in the standard histogram is due to multiple pixel events.

The raw image taken using the Ross pair spectrometer on the same laser shot is shown in Figure 12a and is labeled according to the filters in Table V. The difference in PSL level between two filters of a single Ross pair can be used to estimate the spectrum using Eq. (7) and the residual sensitivities from Table V. The resulting spectrum is given in Fig. 12b. The data point at 40 keV derived from channels 7-8 may be too high due to a possible oxidation layer on the Gd foil in channel 8. However, the other data channels follow a smooth, decreasing Brehmstrallung tail. Since χ is typically larger than the variation in R within a single pass-band, the final error in the derived spectrum is taken to be χ at each energy datapoint. Note the large error bar at 18.5 keV due to the slightly too thin Al foil. The Kα conversion efficiency as measured by the differential filter pair spectrometer was calculated using channels 3-4, since

most of the x-ray energy between 19.99 and 24.35 keV is due to Kα x-rays, and comes out to 1.49×10^{-4}.

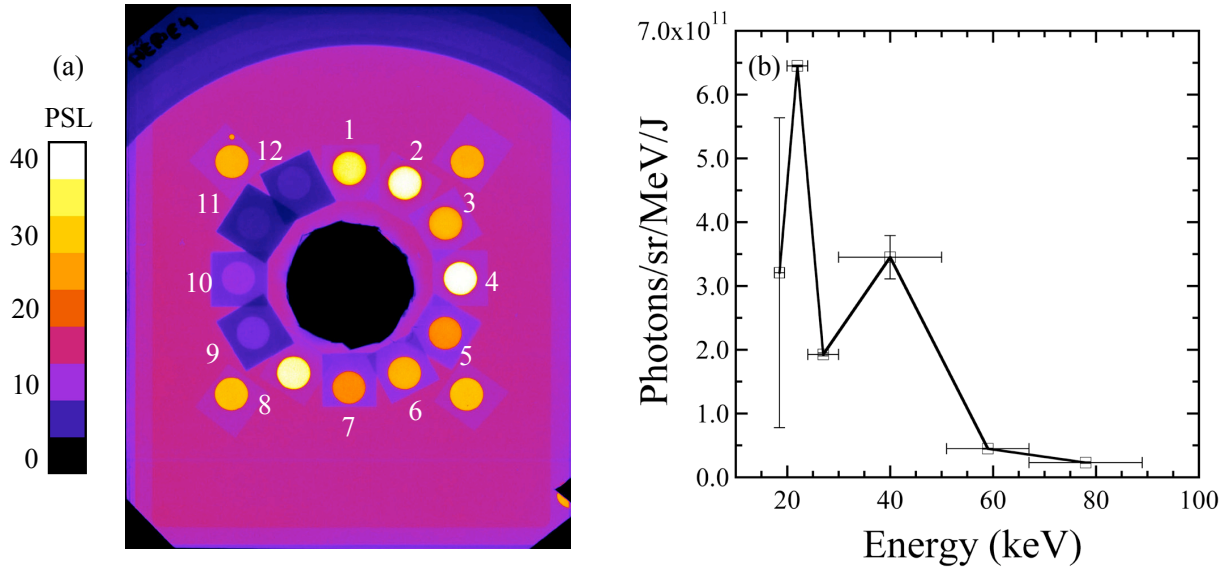

Figure 12. (a) Raw differential filter pair spectrometer image showing channels 1-12 corresponding to the filters in Table III and (b) x-ray spectrum derived from the image data using Eq. (6) and the residual sensitivities from Table V.

Discussion and Conclusions

A six-channel Ross pair spectrometer was designed using calibrated Fuji image plates and fielded to measure the x-ray spectrum and Kα conversion efficiency of a Ag foil petawatt laser-driven backlighter on the Titan laser. The absorption spectrum, spectral sensitivity to x-rays, and image fade rate of image plates was measured and used in the design of the spectrometer. The Kα x-ray conversion efficiency of 1.49×10^{-4} measured by the Ross pair spectrometer using the 19.99 keV – 24.35 keV channel is consistent with previous measurements using the Titan laser at a similar intensity [2]. Although the measurements using a single photon counting CCD were higher by up to a factor of 2, this is likely an overestimate of the conversion efficiency. The counting efficiency of the CCD was based on a calibration at an exposure level

of 21% using monochromatic x-rays and is different for an exposure using a broadband source. This underscores the need to keep exposure levels low when using single photon counting as a diagnostic for petawatt x-ray sources. If the average value of the CCD counting efficiency at 22 keV between 0 and 20% exposure level 0.122% from Ref. [12] is used, then the conversion efficiency using single photon counting comes out to 1.6×10^{-4} with an error of $+/- 0.3 \times 10^{-4}$ based on the standard deviation of the efficiency at 22.162 keV between 0 and 20% exposure level. Further work is required to confirm the spectral shape measured by the Ross pairs, however the good agreement with previously measured Kα conversion efficiencies gives some confidence in the design and calibration.

Acknowledgements

This work was performed under the auspices of the U.S Department of Energy by Lawrence Livermore National Laboratory under Contract No. DE-AC52-07NA27344. Portions of this work were performed at the DuPont-Northwestern-Dow Collaborative Access Team (DND-CAT) located at Sector 5 of the Advanced Photon Source (APS). DND-CAT is supported by E.I. DuPont de Nemours & Co., The Dow Chemical Company and the State of Illinois. Use of the APS was supported by the U. S. Department of Energy, Office of Science, Office of Basic Energy Sciences, under Contract No. DE-AC02-06CH11357.

References

[1] P. Pavan, G. Zanella, and R. Zannoni, *Nucl. Instrum. Meth. Phys. Res. A* **327**, 600 (1993)

[2] H.-S. Park, B. R. Maddox, E. Giraldez, S. P. Hatchett, L. T. Hudson, N. Izumi, M. H. Key, S. Le Pape, A. J. MacKinnon, A. G. MacPhee, P. K. Patel, T. W. Phillips, B. A. Remington, J. F.

Seely, R. Tommasini, R. Town, J. Workman, and E. Brambrink, *Physics of Plasmas* **15**, 072705 (2008)

[3] N. Izumi, R. Snavely, G. Gregori, J. A. Koch, H.-S. Park, and B. A. Remington, *Rev. Sci. Instrum.* **77**, 10E325 (2006)

[4] A. L. Meadowcroft, C. D. Bentley, and E. N. Scott, *Rev. Sci. Instrum.* **79**, 113102 (2008)

[5] H. Ohuchi and A. Yamadera, *Nucl. Instrum. Meth. Phys. Res. A* **490**, 573 (2002)

[6] H. Ohuchi, A. Yamadera, and T. Nakamura, *Nucl. Instrum. Meth. Phys. Res. A* **450**, 343 (2000)

[7] C. Mori and A. Matsumura, *Nucl. Instrum. Meth. Phys. Res. A* **312**, 39 (1992)

[8] M. Ito and Y. Amemiya, *Nucl. Instrum. Meth. Phys. Res. A* **310**, 369 (1991)

[9] J. F. Seely, G. E. Holland, L. T. Hudson, and A. Henins, *Appl. Optics* **47**, 5753 (2008)

[10] S. G. Gales and C. D. Bentley, *Rev. Sci. Instrum.* **75**, 4001 (2004)

[11] M. Sonoda, M. Takano, J. Miyahara, and H. Kato, *Radiology* **148**, 833 (1983)

[12] B. R. Maddox, H.-S. Park, B. A. Remington, and M. McKernan, *Rev. Sci. Instrum.* **79**, 10E924 (2008)

[13] P. A. Ross, *Phys. Rev.* 28, 425 (1926)

[14] I. V. Khutoretsky, *Rev. Sci. Instrum.* **66**, 773 (1995)

[15] C. D. Chen, P. K. Patel, D. S. Hey, A. J. Mackinnon, M. H. Key, K. U. Akli, T. Bartel, F. N. Beg, S. Chawla, H. Chen, R. R. Freeman, D. P. Higginson, A. Link, T. Y. Ma, A. G. MacPhee, R. B. Stephens, L. D. Van Woerkom, B. Westover, and M. Porkolab, *Physics of Plasmas* **16**, 082705 (2009)